energies

MDPI

Article

Assessing Geothermal Energy Production Potential of Devonian Geothermal Complexes in Lithuania

Abdul Rashid Memon and Mayur Pal *

Department of Mathematical Modelling, Faculty of Mathematics and Natural Sciences, Kaunas University of Technology, 44249 Kaunas, Lithuania; abdmem@ktu.lt
* Correspondence: mayur.pal@ktu.lt

Abstract: Lithuania is a Baltic European country which shares borders with Poland, Belarus, Latvia, and Russia and has a geothermal anomaly in the southwestern region. It consists of two main geothermal complexed, i.e., Devonian and Cambrian with a temperature of up to 40 °C (at a depth of 1000 m) and 96 °C (at a depth of 2000 m), respectively. The Devonian complex is composed of an unconsolidated sandstone formation with porosity and permeability in the range of 4–31% and 200 mD–6000 mD, respectively, and these make it a favorable candidate for a low enthalpy geothermal complex because of the high water production rates. This study evaluates the geothermal potential in the Devonian complex of the selected sites for commercial development. The study utilizes the mechanistic modelling approach including uncertainty management to forecast the water production rates and estimate the power generation capacity. Lastly, the study reveals that it is feasible to produce 6 MW to 60 MW of power from the existing vertical wells for a period of 25 years. Furthermore, reactive transport modelling also proves that there is dissolution and precipitation of the minerals near and away from the wellbore, respectively, which impairs the reservoir quality and further concludes that there is an effect of time on re-injection which should be considered to enhance the reservoir quality for future operations. In addition to that, no effect of the re-injection temperature of the produced water is observed.

Keywords: Devonian sandstones; Lithuanian resources; geothermal energy; repurposing wells; screening; numerical modelling; reactive transport modelling

check for updates

Academic Editor: Efstathios E. Michaelides

Received: 13 December 2024
Revised: 13 January 2025
Accepted: 22 January 2025
Published: 28 January 2025

Citation: Memon, A.R.; Pal, M. Assessing Geothermal Energy Production Potential of Devonian Geothermal Complexes in Lithuania. *Energies* **2025**, *18*, 612. https://doi.org/10.3390/en18030612

Copyright: © 2025 by the authors. Licensee MDPI, Basel, Switzerland. This article is an open access article distributed under the terms and conditions of the Creative Commons Attribution (CC BY) license (https://creativecommons.org/licenses/by/4.0/).

1. Introduction

Lithuania is one of three Baltic states and lies on the eastern shore of the Baltic Sea. It shares borders with Latvia to the north, Belarus to the east and south, Poland to the south, and the Russian semi-exclave of Kaliningrad Oblast to the southwest, with a maritime border with Sweden to the west. Lithuania covers an area of 65,300 km^2 (25,200 sq mi), with a population of 2.86 million. Due to EU regulations and zero climate protocol, Lithuania's target to achieve a 45% electricity production from renewable energy sources by 2030 is acknowledged as one of the most ambitious calls within the European Union. The renewable energy sector in Lithuania primarily consists of biomass, biogas, waste-to-energy, hydro, wind, and solar power, with only a small proportion of heating generated by shallow geothermal heat pumps. Geothermal energy possesses the potential to provide a sustainable, equitable, and secure energy supply. The technologies associated with geothermal energy are characterized by low carbon emissions and cleanliness, and they do not encounter the intermittency challenges that are often associated with other renewable energy sources, such as wind and solar power. In Lithuania, the average annual temperature

is between 5 °C and 9 °C, which means people need heating in their homes from October to April. In 2020, Lithuania's total energy consumption was 223,499 TJ with 26% going towards heating and cooling (according to data from the Lithuanian Statistics Department). Of this amount, about 42% (8574.8 GWh) of the heat came from the centralized district heating system.

Lithuania is a major producer of biomass due to the dense forest system; hence, biofuel is used primarily for energy production. Thus, natural gas (27.3%) and biofuel (70.3%) remain the dominant types of fuel in heat production, and no geothermal energy plant contributes towards heat production in Lithuania. The Klaipeda Geothermal Demonstration Plant (KGDP), called "Geoterma", was the first geothermal heating plant in the Baltic Sea region, using 38 °C water from a deep sandstone layer. However, the project faced issues because of a production decline, and it could not compete with the cheaper energy from a nearby incineration plant. These problems almost led to bankruptcy in 2007. Since "Geoterma" closed, there have been no new investments in deep geothermal exploration. The detailed history of the geothermal production is given in reference [1]. Although there are a lot of opportunities for deep geothermal sources, the government does not include any projects on deep geothermal resources.

Lithuania has a geothermal anomaly situated in the southwest of the country and it is related to Middle Proterozoic cratonic granitoid intrusions rich in radiogenic heat producing elements such as Th, U, and K [2]. There are three hydro-geothermal complexes in the sedimentary cover of Western Lithuania: the Cambrian (140 m), Middle-Lower Devonian (400 m), and Upper-Middle Devonian (200 m) [3–6]. In our earlier work [1], we had provided a detailed literature review of the geothermal scenario in Lithuania, while, in reference [7], we had described the workflow analysis, geothermal mechanistic model description, and energy output from the vertical wells for the Cambrian aquifer. Furthermore, in reference [8], we enhanced the power output by redefining the scenarios with the application of horizontal wells. In this article, Devonian sandstone has been selected as the target of the screening study.

The objective of this study is twofold. First, it entails conducting a geological screening of available Devonian geothermal sites within the existing and depleted hydrocarbon reservoirs and other geothermal study areas. Then, numerical modelling will be employed to evaluate the geothermal potential of the selected sites for commercial development. Thus, the main idea of the two-fold study is to create a techno-economic model of the Devonian aquifer site. Similarly, such screening for Cambrian sites has been already carried out earlier and details can be found in reference [7].

In Lithuania, the Devonian reservoir has not extensively studied like Cambrian reservoirs, but only limited sites have been explored and no detailed modelling has been carried out to look at the various production scenarios for a range of properties. Therefore, the culmination of the screening process yields a list of the three most promising geothermal sites. These sites have undergone a detailed analysis involving uncertainty modelling of both dynamic and static parameters. A probabilistic forecasting approach is then applied to estimate the geothermal energy production potential of the Devonian Aquifer [9].

The paper is organized as follows: In Section 2, we first introduce the Devonian geological background under which the study is carried out. Next, we present the data used for the screening of the Devonian Geological sites in Section 3. The modelling methodology and workflow including the criteria for selecting the distance between the doublet pair for geothermal modelling is presented in Section 4. The outcome of the modelling approach used in reference [7] is applied along with the hydrocarbon practice for evaluating high, mid, and low cases for predicting average water production rates. Section 5 presents a reactive transport modelling approach, which is used to test the impact of geothermal fluid

on the reservoir properties. The discussions are presented in Section 6. The conclusions follow in Section 7.

2. Geological Settings of Devonian Strata

Lithuania is located on the Eurasian plateau, at the western edge of the East European Precambrian Craton. The geological section includes Quaternary deposits, Upper Jurassic, Lower Triassic, Upper Permian, Upper, Middle and Lower Devonian, Silurian, and Cambrian [10–13]. The area has three main hydrothermal systems: the Upper-Middle Devonian (D1), Middle-Lower Devonian (D2–3), and Cambrian layers, which are grouped based on their reservoir features. The porosity of these complexes is as follows: 7–15% (C), 20% (D1–2), and 20–24% (D2–3) [14]. At depths between 600 and 900 m lies the second hydro-geothermal system, the Lower-Middle Devonian period, made up of 300–400 m of sandstone and siltstone mixed with clay deposits, with temperatures ranging from 30 °C to 40 °C [15]. Above this is a Middle Devonian layer, 80–100 m thick, made of carbon-rich material. Higher up, at 400–600 m, is the Middle-Upper Devonian hydro-geothermal system, where the temperatures are between 20 °C and 30 °C which is dominated by poorly cemented fine-grained sandstones. This system contains sedimentary rocks up to 200 m thick [2,16–18]. Within this layer, two producing and two injecting wells of the Klaipeda geothermal demonstration heat plant (KGDP) are drilled into this thermal complex and completed at a depth of 1002–1091 m and 975–1118 m, respectively. At the top layer, there are low-temperature waters found in Quaternary deposits, mainly sand and gravel left by glaciers. Figure 1 depicts the geological cross-section of the Lithuanian territory. Table 1 describes the lithology of the Devonian layer from the Kemeri formation. Moreover, sandstone makes up about 70% of the formation. The thickness of the sandstone layers ranges from 2–5 m to 10–18 m. The sandstone is light gray to gray, with grains of varying sizes. It contains feldspar (3.2–6.2%, sometimes up to 16.4%), quartz (69–95%), and small amounts of mica (0.4–1%, occasionally up to 7.4–9.4%). In some areas, the sandstone includes glauconite or siltstone [19]. The sandstone is mostly weakly cemented with clay or dolomitic material [14].

Table 1. Lithology of Devonian Kemeri formation.

Depth m. Below Sea Level	Effective Thickness of Sandstone m	Lithology
820–970	10	Marlstone, dolomite, and fine sandstone
970–980	0	Siltstone, and clay
980–1010	30	Fine sandstone
1010–1035	0	Clay stone
1035–1090	25	Fine sandstone
1090–1130	30	Siltstone, and claystone
>1130		

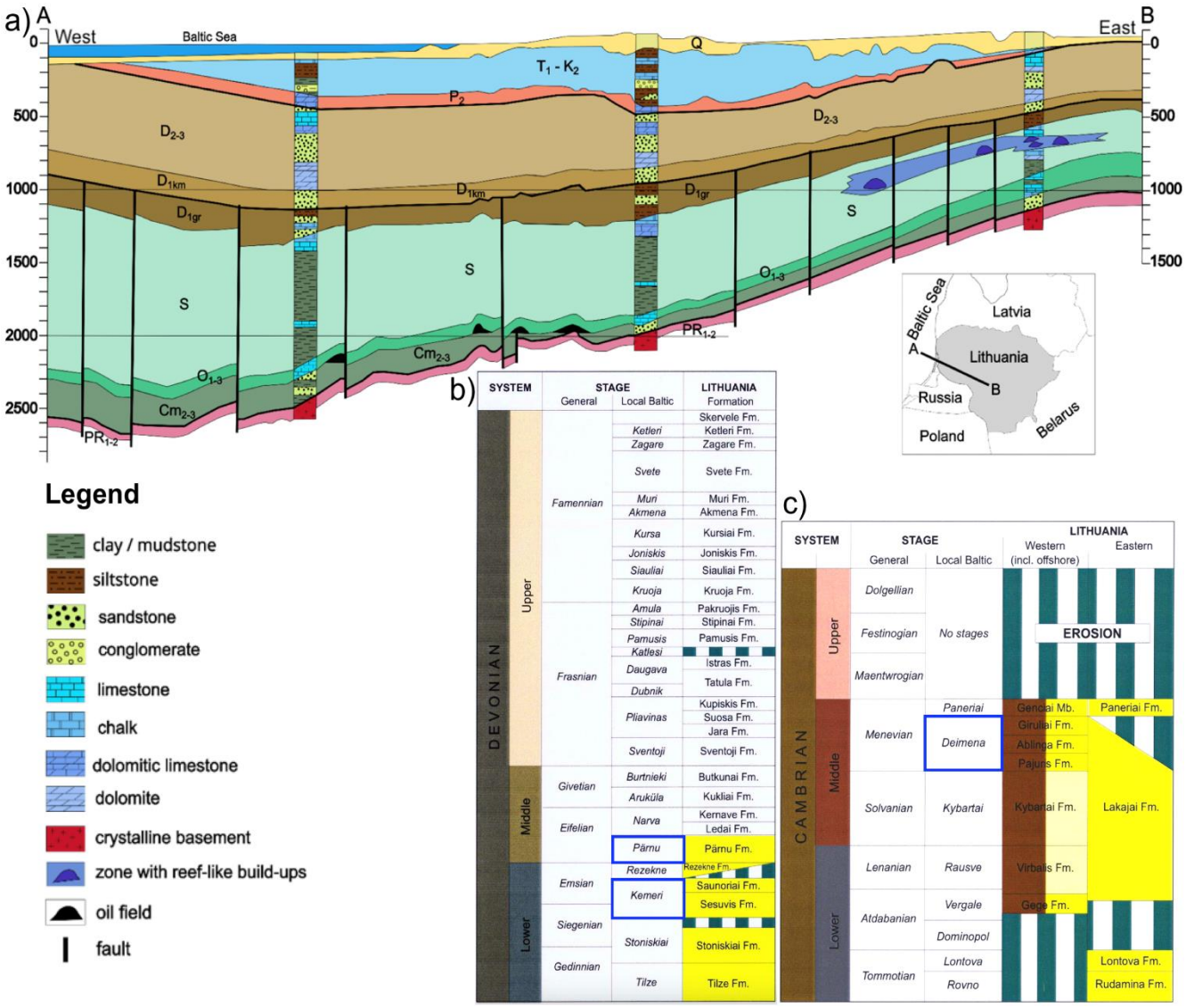


Figure 1. (**a**) Geological cross section of throughout Lithuanian territory (A and B profiles as marked on the Lithuanian map) with Devonian (D) and Cambrian aquifers (cm); and (**b**,**c**) stratigraphic column of Devonian and Cambrian reservoir. The dark brown and yellow color is formation present on the western side and eastern side respectively. While green color represents the erosion of the formation. Investigated intervals are marked in blue [1].

3. Initial Screening of Devonian Sites

As described in the earlier section, Section 1, the Devonian complex has not been fully explored, neither by hydrocarbon industries nor for the geothermal development. There was only one Geothermal Demonstration Plant build in Klaipeda and the history has been summarized in the reference [1]. Moreover, in the KGDP, the production horizon was drilled without core extraction. The geological, petrophysical, and lithological characteristics were assessed based on logging data [20]. The lithological conditions of the Klaipeda wells are inferred from the core analysis of the Vydmantai well. Therefore, based on the extensive literature survey and data availability for geothermal production [21], three promising sites has been screened for the Devonian geothermal model development. The detailed petrophysical properties of the sites are tabulated in the Table 2.

Table 2. Detailed petrophysical properties of the screened sites.

Categories	KGDP I1	Nida	Vydmantai (Devonian)
Name of the structure	Devonian aquifer	Devonian aquifer	2 geothermal wells drilled in Devonian aquifer
Reservoir/Aquifer parameters			
Average Effective porosity, % (min–max)	25; (20.1–31.2)	(11.6–31)	16; (3.747–28.394)
Average permeability, mD (min–max)	2563; (207–6295)	6434; (290–9850)	(207.3–6294.9)
Depth, m	980–1116; 1048	1023–1125.5; 1074	827.6–996.3; 912
Average temperature, °C	38	35–40	34.1
Reservoir thickness, total and effective, m	87; 56	103; 51.5	110.8; 300–115.5
Reservoir Pressure (bars)	109.04	111.72	86 bars at 831 m and 99 bars at 961 m, 95
Net-to-gross (NTG), Units	64		39
Water salinity, mg/L; (density kg/m^3)	92,800; (1067)	80,000–90,000; (1064)	27,600–45,700; (1030)

The compilation of the data has been made from the literature and reports published earlier [6,14,22–24]. The poro-perm data were obtained from the core plugs measurements. The other historical data like pressure and flow rates were obtained from the flow test during the well flow.

4. Modelling Methodology

In this section, we described how the mini models have been developed. First, the petrophysical data have been gathered from the available literature and reports along with the core and log measurements. Then, the dynamic homogenous model was created in T-NAVIGATOR (v21.3-2464-gb2f9b9785f7) from the above measurements to describe the thermal flow and physics simulations [7]. In the initial model development, high, mid, and low cases were developed based on the properties described in Table 2. In geothermal application, the efficiency of the plant depends on the temperature breakthrough in the production well [25]. If the reservoir properties are considerably high, then there are chances of the earlier temperature breakthrough in the vicinity of the production well. Therefore, in the high-case homogeneous reservoir model, simulations were performed using the properties shown in Table 3 to evaluate the thermal breakthrough in high-case scenarios because this information was considered important for deciding the well spacing parameters. Moreover, the ratio of vertical permeability (Kv) to horizontal permeability (Kh) is assumed to be 0.33 for the mid-case scenarios, which represents the most realistic approximation commonly adopted in the oil and gas industry when vertical permeability data are unavailable. Similarly, in low-case and high-case scenarios, this ratio is adjusted by reducing and increasing it by 10%, respectively, resulting in values of 0.30 for the low case and 0.36 for the high case.

Table 3. High-case values of the properties for model development.

Categories	High-Case Values
Porosity (%)	31.2
Permeability (mD)	6295
Kv/Kh, units	0.36
NTG, units	0.64

The next step is to determine the optimal well spacing between the doublet wells [26–28]. In references [1,7,8], we have optimized the well spacing up to 1200 m because the average properties of the Cambrian reservoir were less due to tightness. Therefore, we performed several sensitivities for well spacing, starting from 1200 m and going all the way to 5500 m by increasing the distance between the doublet wells in the T-Navigator 3D reservoir simulator [29]. It was found that the temperature breakthrough occurs quickly

in the production well at a spacing of 1200 m. Figure 2 shows the temperature profile for some of the different well spacing that has been taken under consideration. From Figure 2, it can be observed that no temperature breakthrough in the producer occurs with a well spacing of 5500 m in 25 years. Hence, for all future simulation runs, a similar well spacing of 5500 m is being considered for 25 years for all cases (low/mid/high).

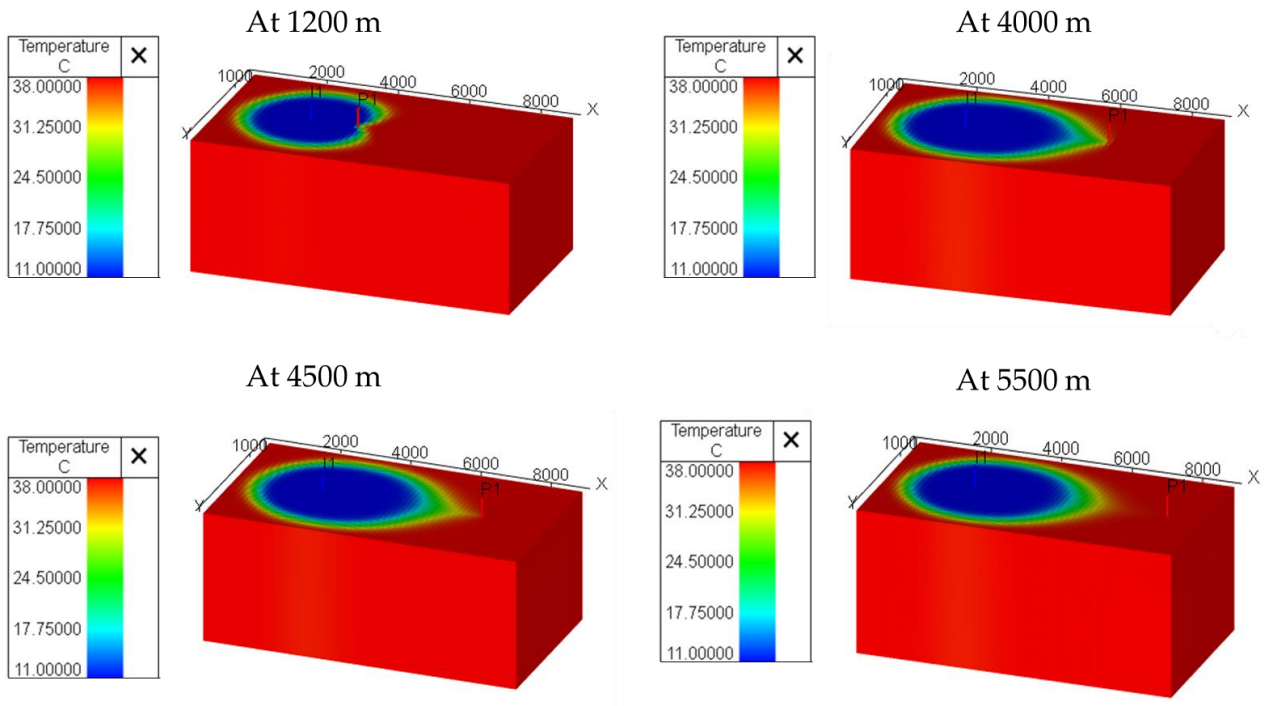


Figure 2. Temperature breakthrough profile for different well spacing less than 5500 m in the doublet wells at the end of 25-year simulation runs.

Once we fixed the well spacing, the next step was to evaluate the full uncertainty on all high, mid, and low cases. For this, we used the experimental design methodology for uncertainty modelling, shown in Figure 3, the details of which are discussed in the next section.

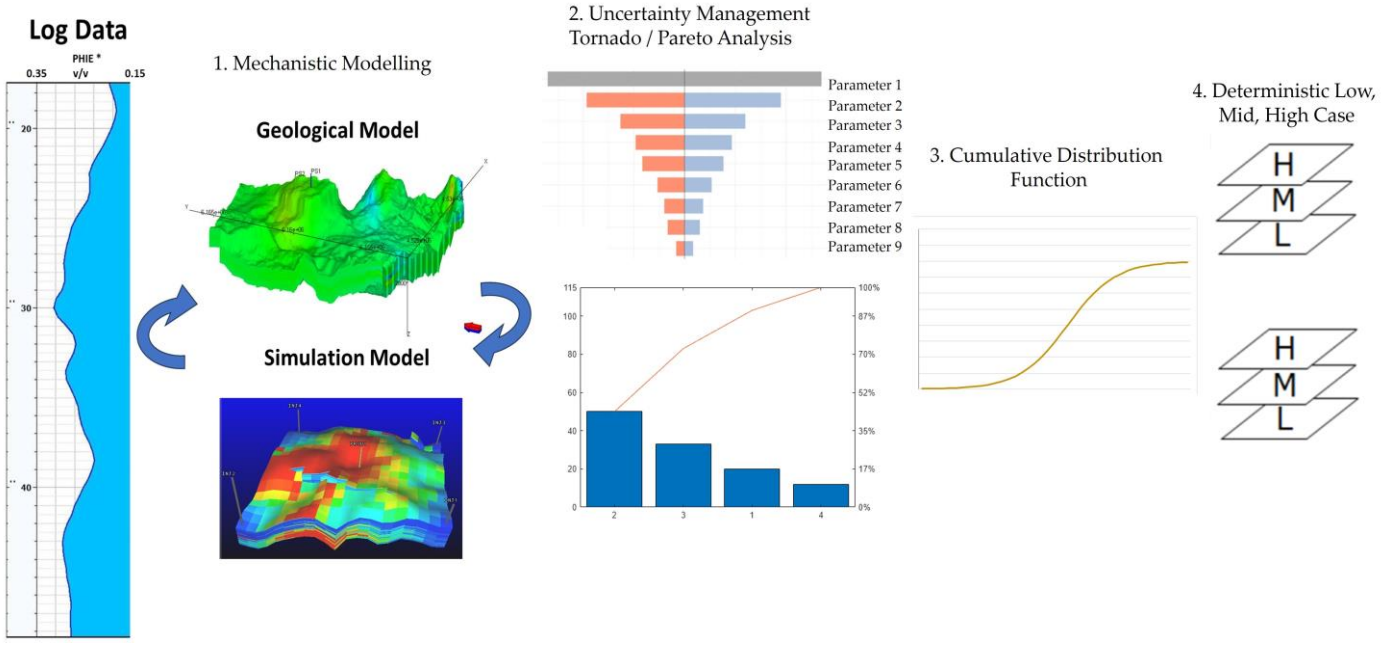


Figure 3. Experimental uncertainty management design workflow.

Uncertainty Analysis Using Experimental Design Workflow

The uncertainty modelling workflow [30] is divided into four key phases, each addressing specific aspects of model development and uncertainty quantification.

In the first phase, the focus is on constructing models with distinct zonation or stratified layers for each producing zone or reservoir layer. These models integrate a comprehensive range of geological and core properties, including porosity, permeability, fluid saturation, and structural features. This process is known as mechanistic modelling, and ensures that the models depict physical and geological realities. However, because the subsurface is inherently complex and the data availability is often limited, uncertainties are introduced at this stage.

The second phase involves addressing these uncertainties by identifying and ranking the parameters that most significantly influence the model's behavior. This is achieved through sensitivity analysis, employing tools such as Tornado charts, which graphically depict the relative impact of each parameter, and Pareto charts, which highlight the cumulative effects of the most critical parameters. These tools facilitate the prioritization of high-impact variables, ensuring that the subsequent analysis focuses on the most influential factors.

In the third phase, the parameters identified as high-ranking in the sensitivity analysis are used to define probability distribution functions (PDFs), which quantify the range and likelihood of their potential values. These distributions are then used in a Monte Carlo simulation, a statistical technique that performs numerous iterations to account for variability and uncertainty in the input parameters. The simulation involves defining input variables, assigning probability distributions to them, and generating thousands or millions of random scenarios. For each scenario, the model computes the result, and the collective outcomes form a probability distribution of possible results. By visualizing the results through histograms, probability distributions, or cumulative curves, decision-makers can assess the risks, plan for uncertainties, and optimize strategies. The outcome of this simulation is a cumulative distribution function (CDF), commonly referred to as an S-curve. The S-curve provides a probabilistic overview of the potential outcomes, illustrating the likelihood of achieving specific performance metrics or resource estimates.

Finally, in the fourth phase, key decision-making metrics are derived from the S-curve. Specifically, the workflow enables the extraction of low (P10), mid (P50), and high (P90) estimates, corresponding to the 10th, 50th, and 90th percentiles of the distribution, respectively. These estimates represent the range of plausible outcomes, with P10 indicating a high-confidence lower limit, P50 reflecting the median or most likely scenario, and P90 indicating a high-confidence upper limit. This phase provides critical inputs for decision-making, planning, and risk assessment, as depicted in Section 4.

This structured workflow ensures a systematic approach to addressing uncertainty, balancing geological realism with statistical rigor to inform robust decision-making in reservoir management. Before moving ahead with the geothermal production potential, the degree of impact of the uncertainty parameters must be evaluated. This uncertainty is solved using the Tornado and Pareto plots.

A Tornado diagram is a straightforward chart that illustrates the sensitivity of the outcomes to variations in individual parameters, one at a time. The chart is called a "tornado" because its shape resembles a funnel or tornado, with the widest bars at the top and the narrowest at the bottom. The variables are arranged in descending order of their impact, making it easy to identify the most influential factors. Each bar represents the range of possible outcomes for a variable when it is varied within its limits, while keeping other variables constant. It also displays the effect of altering each factor while holding all others constant, making it useful for identifying the most impacting factors in each scenario. To construct a Tornado diagram, one must estimate the minimum, average, and

maximum potential values for each factor. The simplicity of Tornado charts makes them highly effective for visualizing complex data. They can also highlight areas where a more detailed investigation or data collection is needed. By focusing on the critical variables, Tornado charts support informed decision-making and help in developing robust strategies for mitigating risks and maximizing outcomes.

On the other hand, the Pareto chart is a basic graphical tool that combines bar and line graphs. Named after the Pareto principle, or the "80/20 rule", it highlights the idea that roughly 80% of effects come from 20% of causes. The bars represent individual values arranged in descending order, while the line indicates the cumulative total of those values. The primary objective of a Pareto chart is to emphasize the most significant parameter among a set of factors. In this chart, bars are ordered from the highest to lowest based on the frequency of occurrence. Consequently, Pareto charts assist in identifying the areas that should be prioritized for improvement. Therefore, the visual simplicity of Pareto charts makes them easy for decision-makers to interpret and communicate. They are a powerful tool for prioritization, helping organizations allocate resources efficiently and achieve maximum impact with minimal effort. More about the Tornado and Pareto experimental workflow can be obtained from reference [7].

Based on the above modelling aspect, we identified the most impacting parameters through sensitivity analysis, and further predictions have been performed. Figure 4 shows the Tornado and Pareto plots of the Devonian aquifer.

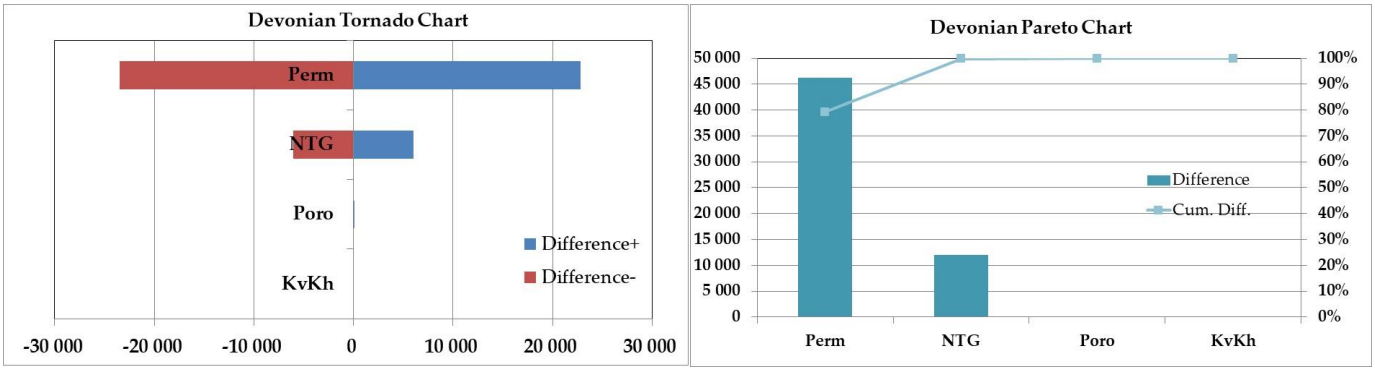


Figure 4. Tornado and Pareto charts of Devonian aquifer.

In Figure 4, the Pareto chart shows a curve representing the cumulative normalized uncertainty. Parameters corresponding to 80% of the full uncertainty (blue dashed line in Pareto chart) are considered the most important impacting parameters (Permeability and Net-To-Gross). The porosity and Kv/Kh have a very minimal impact on the total production rates. Net-to-gross (NTG), porosity, and permeability are interrelated because all three key factors are implied in assessing the quality of a reservoir and its ability to produce fluids effectively. NTG is the ratio of the reservoir rock (net) that has sufficient porosity and permeability to contribute to fluid flow, compared to the total rock volume (gross). A higher NTG indicates a larger proportion of productive rock, while permeability measures the ability of the reservoir rock to allow fluids to flow through it. Thus, rocks with a higher permeability are more effective at transmitting fluids and are more likely to be classified as "net" in the NTG calculation. Conversely, low-permeability layers may be excluded from the "net" category, reducing the NTG. In our case, we cannot see much difference in the minimum and maximum porosity values due to the unconsolidated nature of the reservoir but it shows high differences in the reported permeability values. For the same, Tornado and Pareto charts show a maximum impact of the NTG and Permeability values. Moreover, for heterogenous reservoirs or reservoirs with variable permeability, NTG can help identify the proportion of rock that is productive, aiding in better reservoir

modelling and planning. Furthermore, a reservoir with high NTG and high permeability typically indicates excellent reservoir quality, making it more efficient for water production and high-power outputs for geothermal site selection and better design.

This uncertainty can be well-managed by improving the data quality (like core analysis, well logging and interpretation, and seismic methods) [31], statistical and probabilistic modelling (uncertainty quantification, Monte Carlo simulations, and probabilistic NTG mapping), reservoir characterization (geostatic and facies analysis), dynamic modelling (sensitivity analysis and history matching), scenario planning, and adaptive decision making and risk mitigation.

In our case, we managed the uncertainty by a probabilistic modelling approach. The obtained low- and high-case values of the sensitive parameters (Permeability and NTG) were taken as a property to define several intermediate property values which are created by linear interpolation (Bell Curve) within these two properties to obtain a set of 7. Using this procedure to represent the defined uncertainty range, the likelihood of each set is now evaluated from the normal distribution shown in Figure 5 (Permeability and NTG). This resulted in seven uncertainty ranges for each parameter and generate 7 × 7 cases to be run for the calculation of the average water production rates.

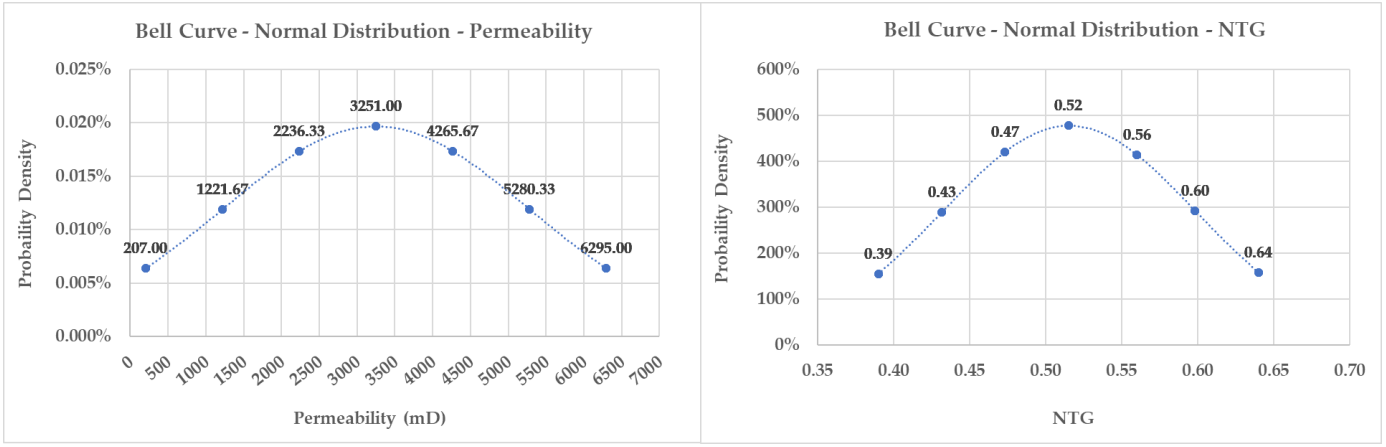


Figure 5. Bell curve of the uncertainty parameters (Permeability and NTG).

Based on the identified values we created high, mid, and low cases to assess the geothermal potential of the Devonian site, which are, therefore, selected for probabilistic water production forecasting—see Table 4.

Table 4. Low-, mid-, and high-case values for Devonian aquifer modelling.

Reservoir Parameters	Devonian Aquifer Parameters
Effective porosity, %	3.75–20–31.2
Permeability, mD	207–3251–6295
Kv/Kh, units	0.30–0.33–0.36
NTG, units	0.39–0.52–0.64

Over 50 simulations were run for the calculation of the average water production rates. Each simulation used a different mix of the uncertainty factors listed earlier. The results are tabulated in Table 5.

Table 5. Average water production based on the sensitivity analysis of Devonian aquifer.

With Porosity Value of 20%—WATER PRODUCTION (Sm^3/day)							
PERMZ	69.00	407.22	745.44	1083.67	1421.89	1760.11	2098.33
PERMX	207.00	1221.67	2236.33	3251.00	4265.67	5280.33	6295.00
NTG							
0.39	1215.93	6974.54	12,575.02	18,102.57	23,573.87	29,015.16	34,382.96
0.43	1344.72	7703.92	13,889.13	19,998.65	26,070.17	32,080.20	38,013.82
0.47	1473.30	8431.12	15,207.63	21,897.01	28,532.00	35,130.60	41,679.67
0.52	1601.74	9158.19	16,515.77	23,791.74	31,004.23	38,191.41	45,350.45
0.56	1730.02	9883.71	17,830.10	25,690.93	33,501.41	41,241.51	48,948.30
0.60	1858.11	10,608.46	19,140.89	27,583.49	35,983.22	44,337.41	52,631.08
0.64	1986.09	11,332.14	20,443.48	29,491.52	38,466.52	47,434.96	56,269.41

From the above analysis, an S-curve for the average water production rates is determined to calculate the low, mid, and high average water production rate as depicted in Figure 6 and the values are tabulated in Table 6. The Devonian aquifer temperature is 38 °C and the re-injection temperature is considered as 11 °C with a temperature difference of 27 °C. The annual average energy production from all different cases is given in Figure 7.

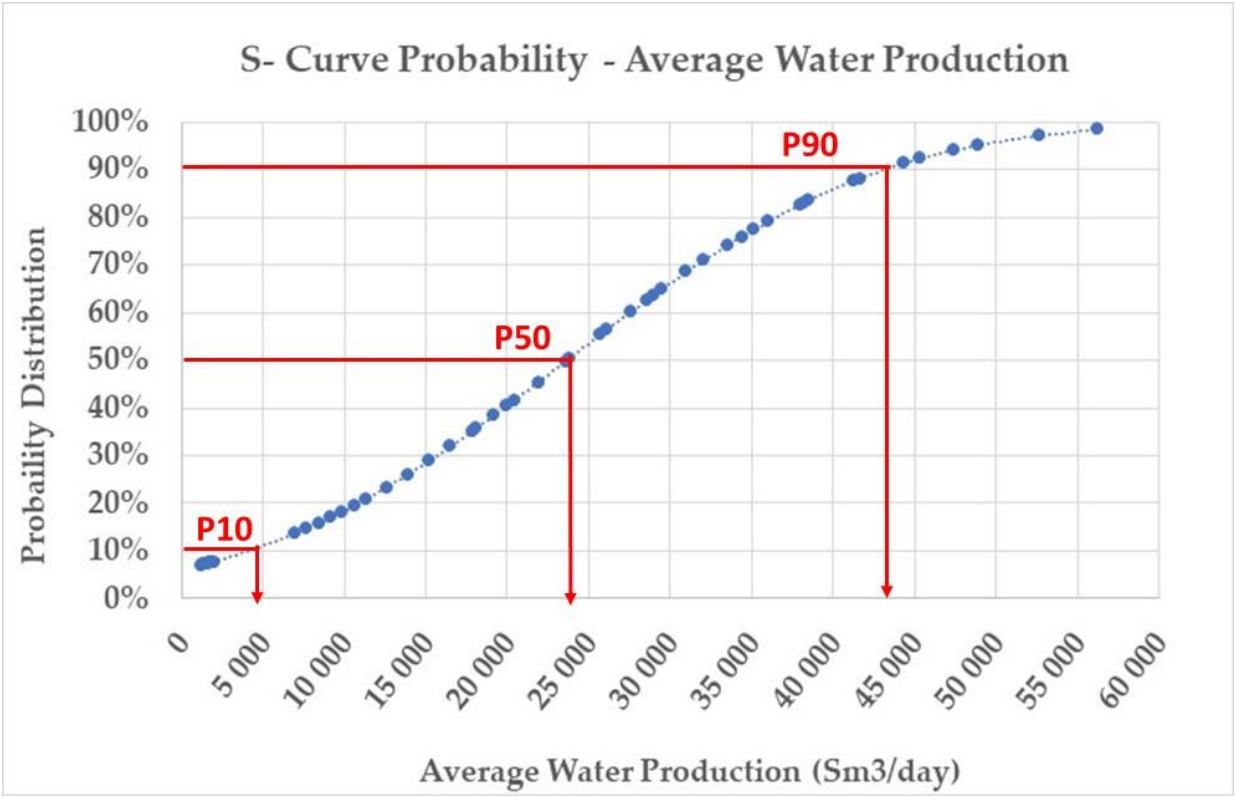


Figure 6. S-curve of average water production rate for Devonian aquifer.

Table 6. Results of subsurface flow modelling of the Devonian aquifer.

Vertical Well Power Calculation Sensitivity—25 Years					
Sr. No	**Case**	**Temperature (°C)**	**Avg. Water Production Rate (Sm^3/day)**	**Energy (GWh)**	**Power (MW)**
1	Low Case	38	4500	1372.05	6
2	Mid Case		23,700	7226.15	33
3	High Case		43,000	13,110.73	60

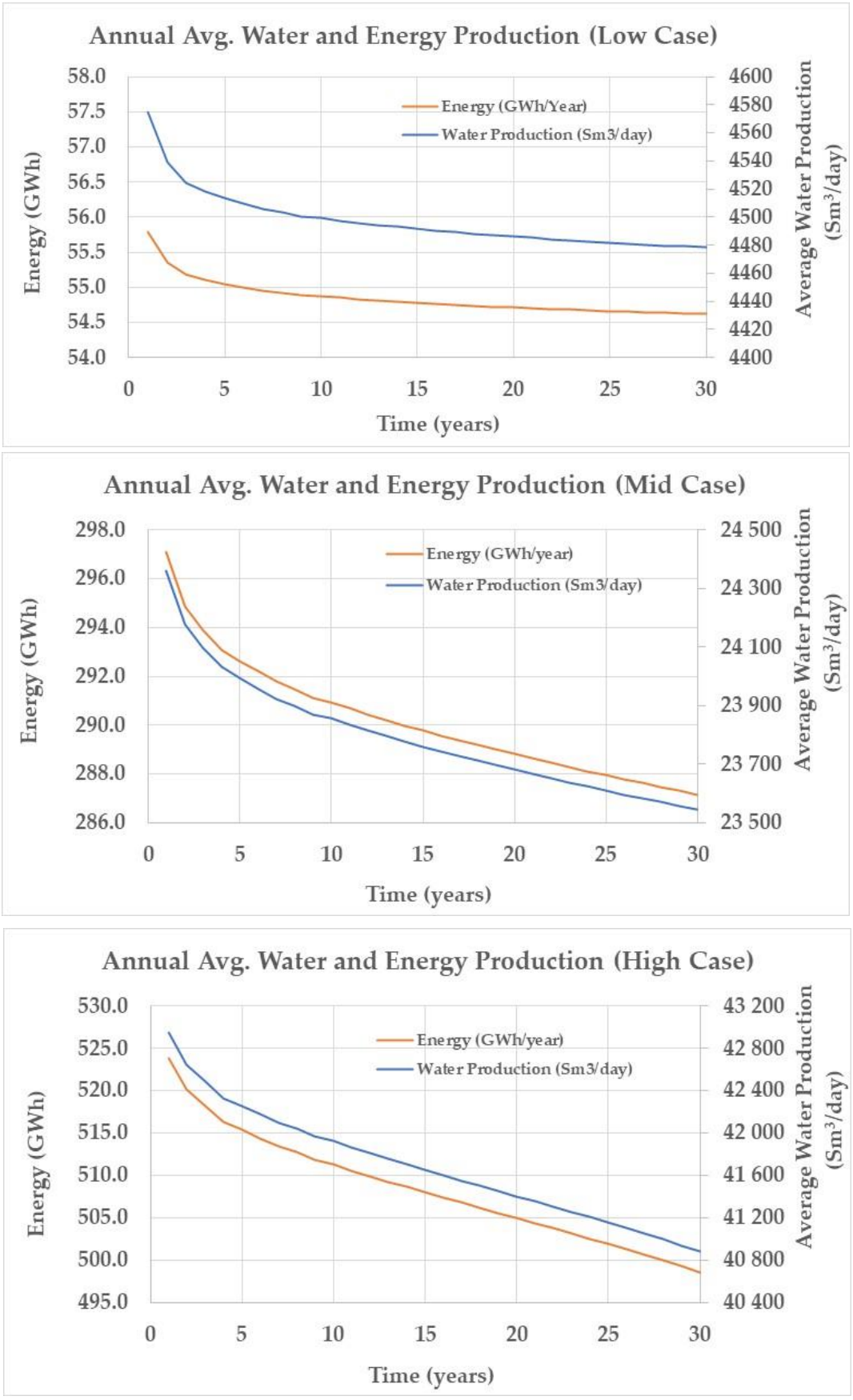


Figure 7. Annual average water and energy production from low, mid, and high case.

5. Reactive Transport Modelling

To gain a comprehensive understanding of the deep geological subsurface, it is essential that we incorporate geological evolutionary modelling to analyze the origins of mineral deposits. This understanding can be significantly enhanced by integrating the geochemical and geothermal interactions at the interfaces between the groundwater flow and dissolution–precipitation processes. A robust framework for this analysis can be achieved through the application of reactive transport modelling. The parameters and interactions encompassed within the reactive transport modelling framework are detailed in Table 7.

Table 7. Reactive transport modelling interfaces [32].

Reactive Transport Coupling	
Geological	site geometry, lithology, and fractures
Thermal	heat loads, and heat flow
Hydrogeological	water pressures, and water flow
Mechanical	rock stress, stiffness, and strength
Chemical	water chemistry, and swelling rocks
Engineering	effects of excavation

In a reactive transport model, geological factors account for the morphology and physical properties of the surrounding rock formations. Engineering considerations are incorporated by analyzing modifications to the geological system, with particular emphasis on the Excavation Disturbed Zone (EDZ) or mining zone. Excavation activities significantly affect the adjacent rock, leading to phenomena such as rock displacement, alterations in stress distribution, and changes in groundwater flow. The region influenced by these changes is referred to as the EDZ. A comprehensive reactive transport model should ideally integrate all six components of the Geological–Thermal–Hydrogeological–Mechanical–Chemical–Engineering (GTHMCE) framework. However, it is not always necessary to develop an all-encompassing model. Instead, the inclusion of interactions should be guided by their potential impact on the model's predictive accuracy and relevance to its specific objectives.

The development and management of geothermal reservoirs primarily aim to devise strategies for the efficient extraction of heat and energy. In Hot Dry Rock (HDR) projects, this process involves the injection of cold water into one borehole, where it flows through the borehole into the hot rock mass and subsequently returns via another borehole. Modelling this system necessitates addressing the intrinsic couplings between several interdependent factors, including in situ stress, the geometry and mechanical–hydrogeological properties of rock fractures, the thermal properties of the rock and water, and the dynamics of water flow.

The objective of this study is to investigate how reactive transport modelling processes, particularly mineral dissolution, interact to predict changes in rock permeability and the transport of minerals through rock structures. The study focuses on understanding the chemical reactions and pressure dissolution mechanisms that influence the permeability of porous and fractured rocks under the combined effects of mechanical and chemical processes. This analysis has been conducted at a large scale using TOUGHREACT simulations (TOUGHREACT_rel_V413_exe_011122) [33]. For this study, a two-dimensional model (2D) was developed to predict the temporal evolution of a reservoir subjected to the re-injection of saline, low-temperature water.

5.1. Effect of Injection Time on the Devonian Reservoir Properties

To study the effect of the injection time, we created a 2D radial model with six uniform layers, each 2.4 m thick, extending 1000 m from the injection well, as shown in the Figure 8. The reservoir's fracture porosity and permeability are listed in Table 8. The heat transfer between the reservoir and the permeable rocks above and below it is an important process.

These confining layers are modeled as endless half-spaces, and the heat exchange is calculated using a semi-analytical method [34]. Table 9 lists the water chemistry and mineral composition of the Devonian aquifer.

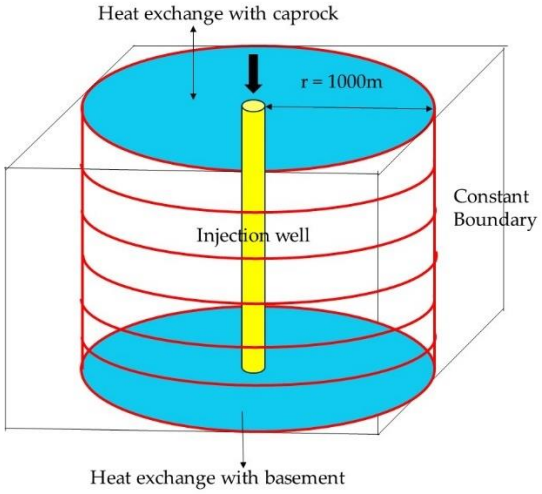


Figure 8. Conceptual model of injection well used in TOUGHREACT (Devonian complex).

Table 8. TOUGH 2 model properties.

Parameters	Model 1	Model 2
Porosity (%)	20	20
Permeability (mD)	300	300
Layers	6	6
Density of water (kg/m^3)	1067	1067
Water re-injection rate (sm^3/day)	5200	28,000
Produced water temperature (°C)	40	40
Re-injection temperature (°C)	11	11
Time period (years)	50	50

Table 9. Water and mineral composition of Devonian aquifer.

Component	Ionic Composition (moles/kg of Water)	Minerals	Chemical Formulae	Fractions
Ca^{+2}	1.03×10^{-3}	Anhydrite	$CaSO_4$	0
Mg^{+2}	1.66×10^{-6}	Calcite	$CaCO_3$	0.004
Na^{+}	1.27×10^{-1}	Anorthite	$CaAl_2Si_2O_8$	0.131
Cl^{-}	1.42×10^{-1}	Illite	$(K,H_3O)(Al,Mg,Fe)_2(Si,Al)_4O_{10}[(OH)_2 \cdot (H_2O)]$	0.054
$SiO_2(aq)$	1.22×10^{-2}	Quartz	SiO_2	0.654
HCO^{3-}	1.04×10^{-3}	Kaolinite	$Al_2Si_2O_5(OH)_4$	0.051
$SO_4{}^{-2}$	2.63×10^{-4}	Muscovite	$KAl_3Si_3O_{10}(OH,F)_2$	0
K^{+}	1.59×10^{-2}	K-feldspar	$KAl_3Si_3O_{10}(OH,F)_2$	0.056
AlO^{2-}	1.08×10^{-5}	Dolomite-2	$[(Mg,Fe)_2SiO_4]$	0.02
Ba^{+2}	1.50×10^{-5}	Celestite	$(SrSO_4)$	0
Sr^{+2}	1.09×10^{-4}	Barite	$BaSO_4$	0
Fe^{+2}	1.02×10^{-2}	Gypsum	$CaSO_4$	0
NH^{4+}	8.10×10^{-3}			
I^{-}	2.83×10^{-3}			
Br^{-}	8.26×10^{-1}			
$B(OH)_3$	2.00×10^{-2}			

Based on the above study, we have analyzed two different scenarios. In the first, we consider a low injection rate (Model 1—5200 sm^3/day), and, in the second, we consider a high injection rate (Model 2—28,000 sm^3/day). The properties of the models used in the simulation, which includes mineral components and their ionic composition and reservoir properties for the Devonian reservoir, are given in Table 8 and the resulting outputs of the simulation are shown in Figures 9 and 10. The changes in reservoir properties, specifically porosity and permeability, are calculated by analyzing the deviation of the counter values from their initial values. This process utilizes the concentration changes legend provided on the right-hand side of the output image for each simulation. Furthermore, the mineral legend indicates the processes of mineral dissolution (represented by negative values) and mineral precipitation (represented by positive values) over the specified time span.

The analysis of Model 1 (low injection rate) indicates that there is a porosity increase near 50 m of radial distance from the well due to the dissolution of minerals and this enhancement increases with time—see Figure 9. Moreover, due to the increment in the porosity near the wellbore, the porosity away from the wellbore decreases by 3.5% due to the mineral deposition within the same period. Similarly, there is a permeability enhancement with time near the wellbore due to mineral dissolution, while, away from the wellbore, the reservoir permeability decreases by 16% due to the mineral deposition within 50 years of time.

Figure 10 presents the analysis of Model 2 (high injection rate), highlighting a progressive increase in porosity within a 50 m radial distance from the well over time. This enhancement is attributed to the mineral dissolution near the wellbore. However, as the porosity increases near the wellbore, it decreases by 3.5% in areas farther from the well within a 50-year period. Similarly, the permeability near the wellbore improves over time due to dissolution, while the permeability farther from the well decreases by 33% over the same period.

These findings indicate that time significantly influences the dissolution and precipitation of minerals within the reservoir. However, beyond a radial distance of 1000 m, the absolute changes in porosity and permeability are negligible.

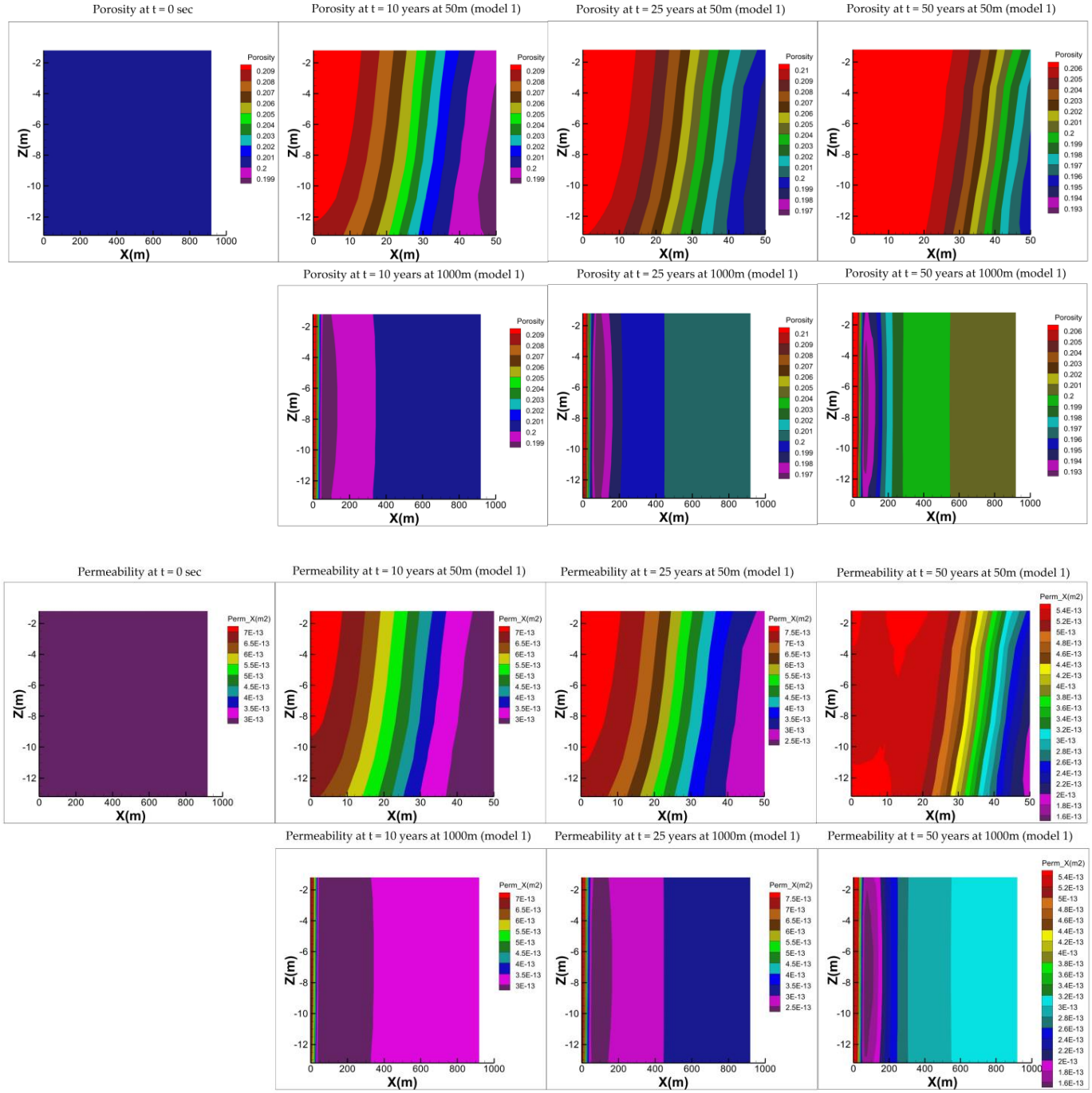


Figure 9. Effect of injection time on the geological properties for Model 1.

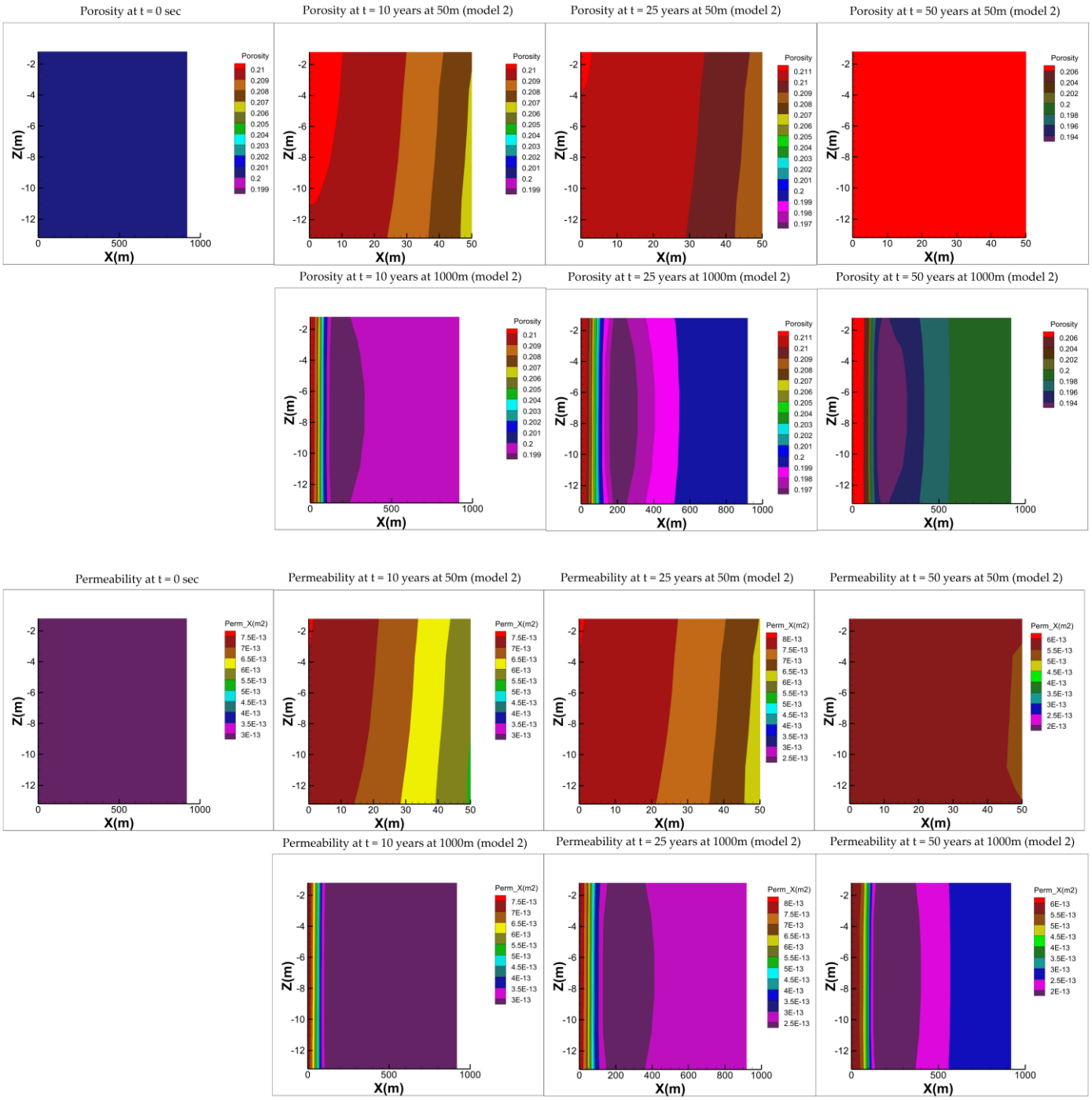


Figure 10. Effect of injection time on the geological properties for Model 2.

5.2. Effect of Injection Rate on the Devonian Reservoir Properties

Figure 11 illustrates the effect of the injection rate on the Devonian complex. The results indicate that increasing the injection rate enhances the reservoir porosity and permeability near the wellbore (within 50 m), with observed increases of 5% and 21%, respectively. However, this dissolution process leads to mineral deposition farther away (at a radial distance of 200 m), resulting in a decrease in the reservoir porosity and permeability by 2.5% and 14%, respectively.

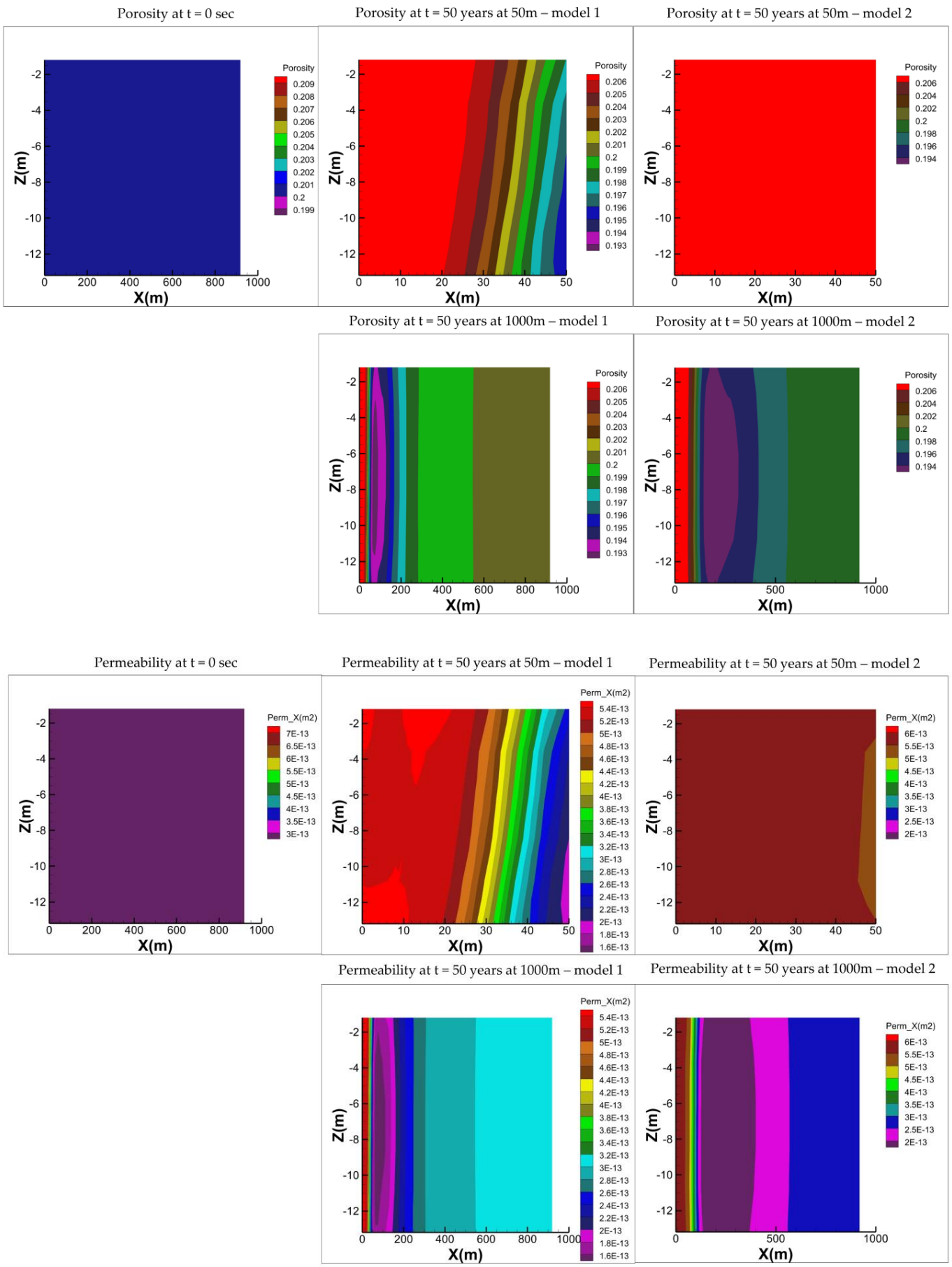


Figure 11. Effect of injection rate on the geological properties for Model 1 and Model 2.

5.3. Effect of Re-Injection Water Temperature on the Devonian Reservoir Properties

This study also examines the impact of the re-injection water temperature on the reservoir properties, as shown in Figure 12. Simulations conducted using Model 1 reveal that the re-injection water temperature has no significant effect on the reservoir parameters or mineral precipitation.

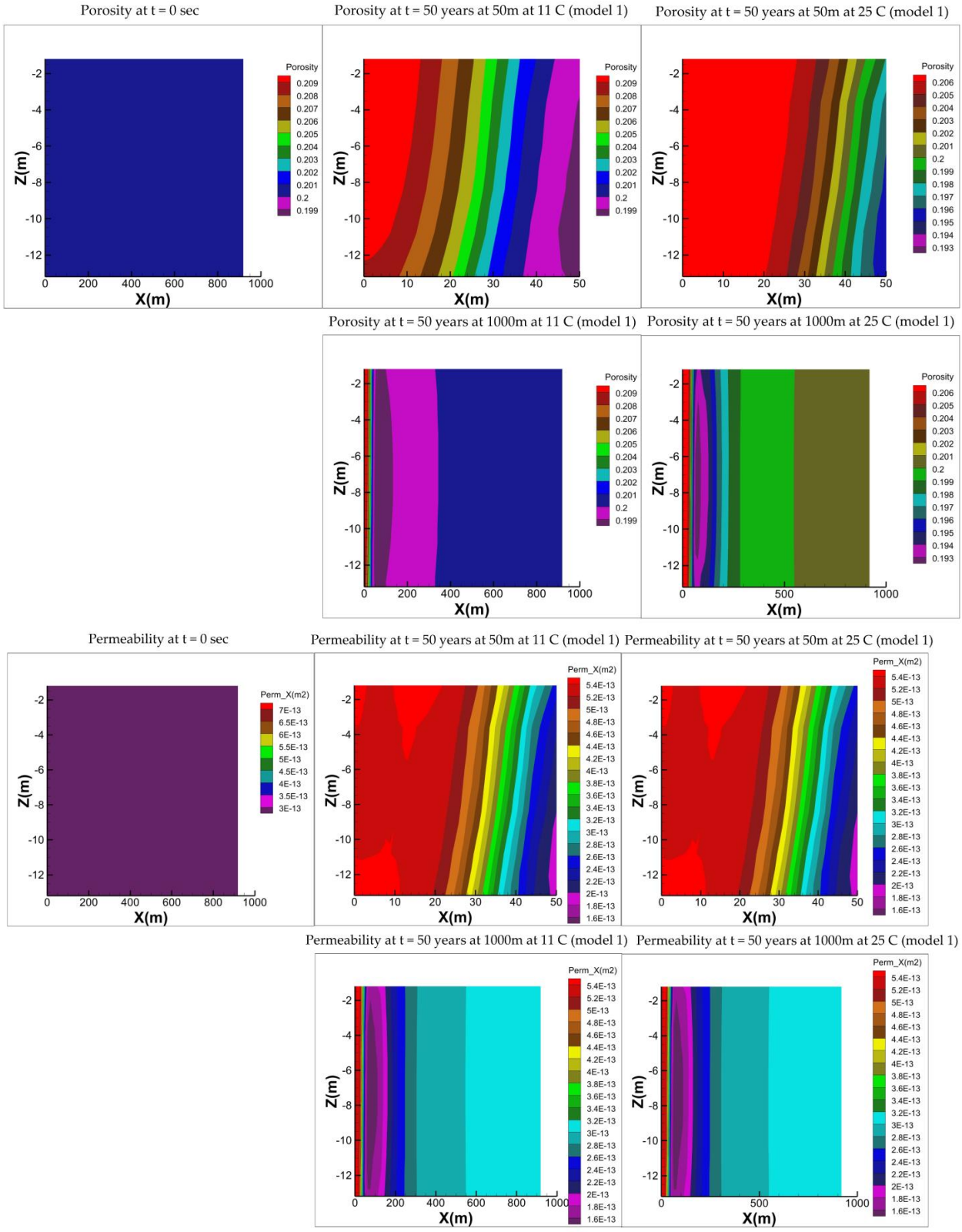


Figure 12. Effect of re-injection water temperature on the reservoir properties for Model 1 and Model 2.

Figure 13 illustrates the dissolution and precipitation patterns of minerals within the Devonian complex for Model 1 and Model 2 over a 50-year timespan. The enhancement in reservoir properties near the wellbore region is primarily attributed to the significant dissolution of Dolomite-2, a mineral containing iron. Among the minerals present, Calcite initially dissolves and subsequently precipitates within the reservoir over the 50-year period. In contrast, minerals such as Anorthite, Illite, Kaolinite, and Dolomite-2 remain in a dissolution phase, while Quartz, Muscovite, and K-feldspar undergo precipitation after 50 years.

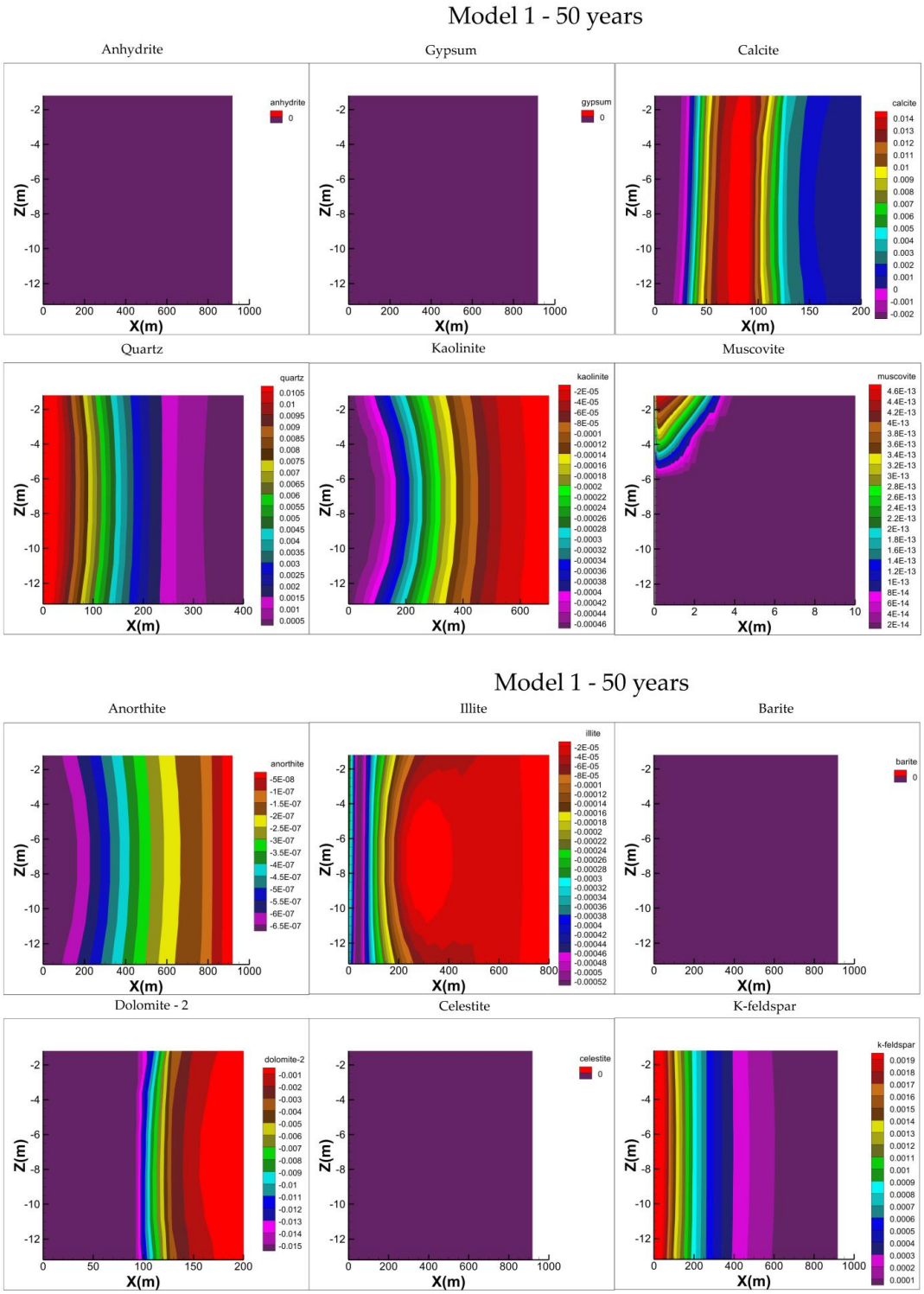


Figure 13. *Cont.*

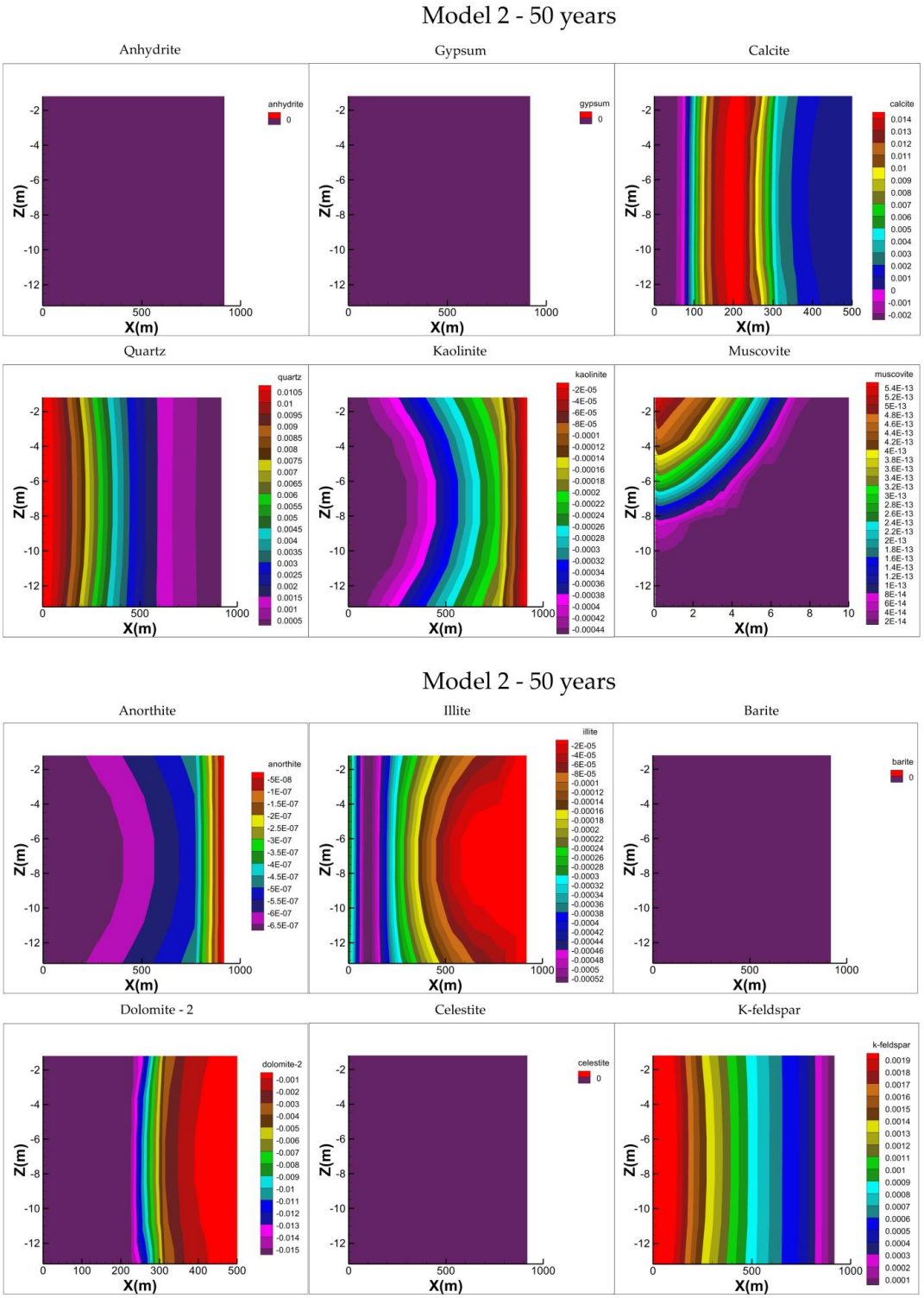


Figure 13. Evolution of mineral dissolution (-ve) and precipitation (+ve) over a time span of 50 years for Model 1 and Model 2.

These findings suggest that prolonged operational timeframes result in intensified mineral dissolution near the wellbore, accompanied by increased mineral deposition further away. This highlights the need for periodic wellbore cleaning to prevent reservoir impairment. Furthermore, the analysis indicates that higher re-injection temperatures do not influence the likelihood of mineral deposition or the impairment of reservoir properties.

6. Discussion

The construction of a 3D reservoir model involves gathering reservoir data, such as well locations, historical injection/production records, porosity and permeability, and mineral deposition, and this was difficult due to the non-availability of data for some of the sites. To address this issue, uncertainty principles are used in this study. The permeability values provided were mostly for gas permeability or log estimates. There was also a common assumption that the porosity was effective porosity rather than total porosity. This suggests a lack of standardized reporting practices. Moreover, the reported values often varied across sources, including different measurement systems. In our case, the modelling process did not include seismic data, but, instead, used simple box models with randomly generated distributions based on average geological properties. The determination of the well spacing is also based on the homogenous properties of the model which should be given more consideration if the reservoir is heterogenous. Hence, a future collection of field data and a relevant study would be needed to address the remaining gaps.

One limitation of this study is the reliance on 3D mechanistic models for doublet spacing and geothermal reservoir modelling. While these models are relatively easy to construct and facilitate a rapid uncertainty analysis, they lack the comprehensive detail of a fully integrated modelling approach. Such an approach would involve tying the log data and reservoir data to seismic data and performing history matching with the well production data. Developing a fully detailed model for the final selected site represents an area for future work.

Moreover, mineral data regarding precipitation have been collected from reports that were available. Based on that, a reactive transport model was developed to properly analyze the injection fluid temperature and recommendations have been made including the effect of the time and temperature on determining the re-injection strategy. Therefore, a future geochemical study would be needed to address the remaining gaps.

Thus, the main challenges associated are exploration and production challenges which include an increased sand cementation with depth and temperature, along with the highly variable thickness and permeability of the Devonian layer, which makes predictions difficult until drilling occurs. This creates challenges in estimating the potential flow rates, especially when reworking old wells or drilling new ones, and includes the data assimilation of water chemistry. Many sites like Klaipeda lack detailed information about underground formations for future geothermal development.

7. Conclusions

In accordance with the well spacing and geological screening criteria, 3D models were developed for the designed site (the Devonian aquifer). The findings indicated that, with a well spacing of 5500 m, it is theoretically feasible to produce heat at a rate of 1370 to 13,100 GWh (a power output of 6 MW to 60 MW). The analysis underscores the significance of both the water temperature and production rate in determining the geothermal potential of each site over a 25-year period. The high power production is due to the high average water production rates, which is due to the increased permeability.

Reactive transport modelling (2D) reveals that mineral dissolution predominantly occurs near the wellbore region, while mineral precipitation is observed further away. These mineralogical changes lead to an increase in porosity and permeability within 50 m of the wellbore, accompanied by a decrease in reservoir porosity and permeability in regions farther from the wellbore. Additionally, the re-injection temperature has minimal impact on reservoir properties. However, over extended time spans (10, 25, and 50 years), the intensity of mineral dissolution near the wellbore increases, while precipitation progressively intensifies further from the wellbore.

Finally, this study shows that it is possible to further develop the Devonian sites for geothermal purposes. Different possibilities are shown with help of low-, mid-, and high-case scenarios of such development. This study also shows that the issues related to the flow rates and injectivity can be tackled using a better well configuration and design. The reactive transport model helps to build awareness about the mineral dissolution and precipitation issues in geothermal systems, which can help in the development of better operating principles including the use of chemical inhibitors and technologies to deal with such issues.

Author Contributions: Conceptualization, A.R.M. and M.P.; methodology, A.R.M. and M.P.; software, A.R.M.; validation, M.P.; formal analysis, A.R.M. and M.P.; investigation, A.R.M.; resources, A.R.M.; data curation, A.R.M.; writing—original draft preparation, A.R.M. and M.P.; writing—review and editing, A.R.M. and M.P.; visualization, A.R.M.; supervision, M.P.; project administration, M.P.; funding acquisition, M.P. All authors have read and agreed to the published version of the manuscript.

Funding: This project has received funding from the Research Council of Lithuania (LMT), Agreement No. P-MIP-23-102.

Data Availability Statement: The original contributions presented in this study are included in the article. Further inquiries can be directed to the corresponding author.

Acknowledgments: The authors would to express thanks for the LMT funding from Project No. P-MIP-23-102 for supporting the research work presented in this paper. The authors would also like to thank Klaipeda Energy and Minijos Nafta for the subsurface insights during the course of this work. The authors would also like to acknowledge the support from Pijus Makauskas and Ieva Kaminskaite-Baranauskiene for their valuable contributions during the development of the models and reactive transport modelling.

Conflicts of Interest: The authors declare no conflicts of interest.

References

1. Memon, A.R.; Makauskas, P.; Kaminskaite-Baranauskiene, I.; Pal, M. Unlocking Geothermal Energy: A Thorough Literature Review of Lithuanian Geothermal Complexes and Their Production Potential. *Energies* **2024**, *17*, 1576. [CrossRef]
2. Šliaupa, S.; Motuza, G.; Korabliova, L.; Ciuraite, K.; Puronas, V. Geothermal potential of hot granites of Lithuania. In Proceedings of the World Geothermal Congress 2010, Bali, Indonesia, 25–29 April 2010.
3. Zuzevičius, A.; Jurevičius, A.; Galčiuvienė, K. The Geoenvironmental Impact of Klaipėda Geothermal Plant. *J. Environ. Eng. Landsc. Manag.* **2011**, *19*, 304–315. [CrossRef]
4. Klimas, A.A.; Gregorauskas, M.; Malisauskas, A. Computer Models, Used for Klaipeda Geothermal Plant Operation Failures Analyse. *Rigas Teh. Univ. Zinat. Rak.* **2010**, *45*, 7–15.
5. Radeckas, B.; Lukosevicius, V. Klaipeda Geothermal Demonstration Project. In Proceedings of the World Geothermal Congress 2000, Kyushu-Tohoku, Japan, 28 May–10 June 2000; pp. 3547–3550.
6. Zinevicius, F.; Sliaupa, S. Lithuania—Geothermal Energy Country Update. In Proceedings of the World Geothermal Congress 2010, Bali, Indonesia, 25–29 April 2010.
7. Makauskas, P.; Kaminskaite-Baranauskiene, I.; Memon, A.R.A.N.; Pal, M. Assessing Geothermal Energy Production Potential of Cambrian Geothermal Complexes in Lithuania. *Energies* **2024**, *17*, 1054. [CrossRef]
8. Memon, A.R.A.N.; Makauskas, P.; Kaminskaite-Baranauskiene, I.; Pal, M. Workflow for Assessing Geothermal Potential of Depleted Hydrocarbon Fields: A Study of Cambrian Reservoirs in Lithuania. In Proceedings of the European Association of Geoscientists & Engineers, Oslo, Norway, 2–5 September 2024; ECMOR: Oslo, Norway, 2024; pp. 1–13. [CrossRef]
9. Laugier, B.; Aming, A. Unsupervised AI Workflow to Evaluate CO_2 Storage and Geothermal Potential Over a Giant Mature Gas Field. In Proceedings of the Third EAGE Workshop on HPC in Americas, Online, 17–18 May 2022.
10. Brehme, M.; Nowak, K.; Banks, D.; Petrauskas, S.; Valickas, R.; Bauer, K.; Burnside, N.; Boyce, A. A Review of the Hydrochemistry of a Deep Sedimentary Aquifer and Its Consequences for Geothermal Operation: Klaipeda, Lithuania. *Geofluids* **2019**, *2019*, 4363592. [CrossRef]

11. Brehme, M.; Blöcher, G.; Regenspurg, S.; Milsch, H.; Petrauskas, S.; Valickas, R.; Wolfgramm, M.; Huenges, E. Approach to develop a soft stimulation concept to overcome formation damage—A case study at Klaipeda, Lithuania. In Proceedings of the 42nd Workshop on Geothermal Reservoir Engineering, Stanford, CA, USA, 13–15 February 2017; Stanford University: Stanford, CA, USA, 2017.
12. Brehme, M.; Regenspurg, S.; Leary, P.; Bulut, F.; Milsch, H.; Petrauskas, S.; Valickas, R.; Blöcher, G. Injection-Triggered Occlusion of Flow Pathways in Geothermal Operations. *Geofluids* **2018**, *2018*, 4694829. [CrossRef]
13. Klemetsdal, Ø.; Nilsen, H.; Krogstad, S.; Andersen, O.; Bastesen, E. Modeling and Optimization of Shallow Geothermal Heat Storage. In Proceedings of the European Conference on the Mathematics of Geological Reservoirs, The Hague, The Netherlands, 5–7 September 2022.
14. Zinevicius, F.; Rasteniene, V.; Bickus, A. Geothermal Development in Lithuania. Available online: https://pangea.stanford.edu/ERE/pdf/IGAstandard/EGC/szeged/O-4-07.pdf (accessed on 1 September 2023).
15. Suveizdis, P.; Rasteniene, V.; Zinevicius, F. Geothermal Potential of Lithuania and Outlook for Its Utilization. In Proceedings of the World Geothermal Congress 2000, Kyushu-Tohoku, Japan, 28 May–10 June 2000.
16. Šliaupa, S.; Zinevičius, F.; Mazintas, A.; Petrauskas, S.; Dagilis, V. Geothermal Energy Use, Country Update for Lithuania. In Proceedings of the European Geothermal Congress, Den Haag, The Netherlands, 11–14 June 2019.
17. Šliaupa, R.S.; Zuzevičius, A.; Rastenienė, V.; Baliukevičius, A.; Zinevičius, F.; Gudzinskas, J. Vakarų Lietuvos Regione Esančių Geoterminės Energijos Resursų Potencialo Išaiškinimas ir Pagrindimas, bei Galimybės jų Panaudojimui Energijos Gamybai. 2008. Available online: https://enmin.lrv.lt/uploads/enmin/documents/files/Veikla/Veiklos%20sritys/Atsinaujinantys%20energijos%20%C5%A1altiniai/Moksliniai-tiriamieji%20darbai/Geotermines_energijos_potencialas.pdf (accessed on 1 January 2025).
18. Malik, S.; Makauskas, P.; Sharma, R.; Pal, M. Exploring CO_2 storage potential in Lithuanian deep saline aquifers using digital rock volumes: A machine learning guided approach. *Balt. Carbon Forum* **2023**, *2*, 13–14. [CrossRef]
19. Puronas, V. A Reservoir Model and Production Capacity Estimate for Cambrian Geothermal Reservoir in Kretinga, Lithuania. In *Geothermal Training Programme, Orkustofnun, Grensásvegur 9, IS-108 Reykjavík, Iceland. Reports*; United Nations University: Shibuya, Japan, 2002; Number 11; pp. 187–204.
20. Parent, A.; Vogt, C.; Bonomi, C.; Fuchs, T.; Schulze-Riegert, R.; Krzikalla, F.; Carles, M.; Lipinski, B. Geothermal Rapid Screening. In Proceedings of the 3rd EAGE Global Energy Transition Conference and Exhibition, The Hague, The Netherlands, 7–9 November 2022.
21. Petrauskas, S.; Šliaupa, S.; Nair, R.; Valickas, R. *The Horizon 2020 SURE Project: Deliverable 6.1—Field Scale RJD Stimulation for the Klaipeda Site*; GFZ German Research Centre for Geosciences: Potsdam, Germany, 2019.
22. Zinevicius, F.; Bickus, A.; Rasteniene, V.; Suveizdis, P. Geothermal Potential and First Achievements of its Utilization in Lithuania. In Proceedings of the World Geothermal Congress 2005, Antalya, Turkey, 24–29 April 2005.
23. Guinot, F.; Marnat, S. Death by Injection: Reopening the Klaipėda Geothermal Cold Case. In Proceedings of the 46th Workshop on Geothermal Reservoir Engineering, Stanford, CA, USA, 15–17 February 2021; Stanford University: Stanford, CA, USA, 2021.
24. Suveizdis, P.; Rasteniene, V.; Zui, V. Geothermal field of the Vydmantai-1 borehole within the Baltic heat flow anomaly. *Baltica* **1997**, *10*, 38–46.
25. Rivera Diaz, A.; Kaya, E.; Zarrouk, S.J. Zarrouk. Reinjection in Geothermal Fields: A Worldwide Review Update. In Proceedings of the World Geothermal Congress 2015, Melbourne, Australia, 19–25 April 2015.
26. Schulze-Riegert, R.; Davies, R.; Coronado, J.; Hug, C.; Joonnekindt, J.P.; Mulyani, S.; Pradana, A.; Intani, R.G.; Golla, G.; Gunderson, R.; et al. Well Placement Optimization for Geothermal Reservoirs Under Subsurface Uncertainty. In Proceedings of the European Conference on the Mathematics of Geological Reservoirs 2022, The Hague, The Netherlands, 5–7 September 2022.
27. Kong, Y.; Pang, Z.; Shao, H.; Kolditz, O. Optimization of well-doublet placement in geothermal reservoirs using numerical simulation and economic analysis. *Environ. Earth Sci.* **2017**, *76*, 118. [CrossRef]
28. Watson, S.M.; Falcone, G.; Westaway, R. Repurposing Hydrocarbon Wells for Geothermal Use in the UK: The Onshore Fields with the Greatest Potential. *Energies* **2020**, *13*, 3541. [CrossRef]
29. T-Navigator—Geothermal Modelling Software from Rock Flow Dynamics. Available online: https://rfdyn.com/solutions/new-energy/ (accessed on 1 January 2025).
30. Hoteit, H.; He, X.; Yan, B.; Vahrenkamp, V. Uncertainty quantification and optimization method applied to time-continuous geothermal energy extraction. *Geothermics* **2023**, *110*, 102675. [CrossRef]
31. Sanyal, S.K.; Morrow, J.W. An investigation of drilling success in geothermal exploration, development and operation. *Geothermal. Resour. Counc. Trans.* **2011**, *35*, 233–237.
32. Andersson, J.; Hudson, J.A. *T-H-M-C Modelling of Rock Mass Behaviour—1: The Purposes, the Procedures and the Products*; Geo-Engineering Book Series; Elsevier: Amsterdam, The Netherlands, 2004; Volume 2, pp. 433–438. [CrossRef]

33. Sonnenthal, E.; Spycher, N.; Xu, T.; Zheng, L. TOUGHREACT V4. 12-OMP and TReactMech V1. 0 Geochemical and Reactive-Transport User Guide. 2021. Available online: https://escholarship.org/uc/item/8945d2c1 (accessed on 1 January 2025).
34. Xu, T.; Sonnenthal, E.; Spycher, N.; Zheng, L.; Miller, N.; Pruess, K. Toughreact V3. 0-OMP Sample Problems. Lawrence Berkeley National Laboratory-Earth & Environmental Sciences. 2014. Available online: https://tough.lbl.gov/assets/docs/TOUGHREACT_V3-OMP_SampleProblems.pdf (accessed on 1 January 2025).

Disclaimer/Publisher's Note: The statements, opinions and data contained in all publications are solely those of the individual author(s) and contributor(s) and not of MDPI and/or the editor(s). MDPI and/or the editor(s) disclaim responsibility for any injury to people or property resulting from any ideas, methods, instructions or products referred to in the content.